Hierarchical Mechanochemical Switches in Angiostatin

Fabio Grandi,[a] Massimo Sandal,[a] Giovanni Guarguaglini,[a, b] Emidio Capriotti,[c] Rita Casadio,[c] and Bruno Samorì*[a, b]

We wish to propose a novel mechanism by which the triggering of a biochemical signal can be controlled by the hierarchical coupling between a protein redox equilibrium and an external mechanical force. We have characterized this mechanochemical mechanism in angiostatin, and we have evidence that it can switch the access to partially unfolded structures of this protein. We have identified a metastable intermediate that is specifically accessible under thioredoxin-rich reducing conditions, like those met by angiostatin on the surface of a tumor cell. The structure of the same intermediate accounts for the unexplained antiangiogenic activity of angiostatin. These findings demonstrate a new link between redox biology and mechanically regulated processes.

Introduction

The extent and fate of many biological processes are drastically affected by the stresses and strains that are exerted during their development.[1–3] To understand the behavior of these processes, force as a physical variable must also be taken into account.[4] A mechanical tension can alter the functional states of proteins and activate processes. In the case of PECAM-1 for instance, mechanical tension switches on the binding of this protein with a kinase.[5] Likewise, it promotes the exposure of binding sites that serve as nucleation centers for the self-assembly fibronectin into a fibrillar form.[6]

Disulfide bonds are believed to have been added during evolution to enhance the stability of proteins that function in fluctuating cellular environments. Recent evidence indicates that disulfide bonds can be more than inert structural motifs and that they can act as switches for different protein functions.[7] The switching capabilities of the coupling of disulfide redox equilibria with a mechanical force have been addressed by Discher and colleagues in a vascular cell-adhesion protein.[8] The chemical kinetics of disulfide reduction under an external force have been more recently investigated by Fernandez and colleagues.[9]

Angiostatin (ANG) is a multimodular protein that contains disulfide bonds and is located on the basement membrane where different reductases are present,[10] and mechanical stretching forces are constantly being developed.[11] This combination of mechanochemical stress and redox conditions in the in vivo ANG environment makes this protein an ideal model system for addressing the issue of the possible triggering of biochemical signals by the combination of mechanochemical forces and redox equilibria.

ANG is an extracellular fragment of plasminogen, and is composed of five highly homologous, tandem kringle domains (K1–K5). All of them contain three internal disulfide bonds, which define a triple-loop topology like that displayed in Figure 1.[12] It is in clinical trials as an antitumor agent because of its ability to inhibit angiogenesis.[13, 14] However, the determination of the inhibition mechanism at the molecular level remains a very open challenge.
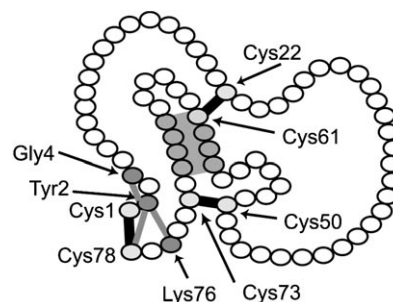
Figure 1. The triple-loop topology of an ANG kringle domain (K4) defined by the three internal disulfide bonds (black). The two critical noncovalent interactions that control the mechanochemical unfolding of the ANG domains are the hydrogen bonds connecting the N and C termini (light gray) and a short β-sheet.

[a] F. Grandi,+ M. Sandal,+ G. Guarguaglini, Prof. B. Samorì
Department of Biochemistry, University of Bologna
Via Irnerio 48, 40126 Bologna (Italy)
Fax: (+39)51-2094387
E-mail: samori@alma.unibo.it

[b] G. Guarguaglini, Prof. B. Samorì
National Center of Nanostructures and bioSystems at Surfaces (S3) of INFM
Via G.Campi 2, 41100 Modena (Italy)

[c] E. Capriotti, Prof. R. Casadio
CIRB Laboratory of Biocomputing, Department of Biology
University of Bologna
Via Irnerio 42, 40126, Bologna (Italy)

[+] These authors contributed equally to this work.

Supporting information for this article is available on the WWW under http://www.chembiochem.org or from the author.

These are not the final page numbers! ↗↗

Here we show how redox and mechanical switches can be coupled in ANG to generate a higher level of switching complexity.

Results and Discussion

ANG acts within the extracellular matrix (ECM).[15] It also binds cell-surface receptors, like focal adhesion integrin $\alpha_v\beta_3$, angiomotin and cell-surface F1-ATPase (ref. [16] and references therein) in actively migrating endothelial cells. In this environment, stresses of the order of $5.5\ \text{nN}\,\mu\text{m}^{-2}$ are generated.[17] It has been proven that these stresses are able to unfold ECM multimodular proteins, like fibronectin.[3] Because of the covalent disulfide bonds in its kringle domains (Figure 1), ANG can be mechanically unfolded under those stresses only under reducing conditions. Incubation of ANG with increasing concentrations of a reducing agent, like dithiothreitol (DTT) leads to the reduction and sequential opening of its internal disulfide bonds in the different domains: first, Cys1–Cys78 only, then Cys22–Cys61 and Cys50–Cys73, in sequence, as reported in a previous paper.[18]

We have studied the mechanical unfolding of the ANG domains in their different redox states at the simulation level by the steered molecular-dynamics (SMD) approach,[19] and at the experimental level by new experiments following the single-molecule force spectroscopy (SMFS) methodology, which is based on atomic force microscopy (AFM).[18, 20–25] Because of the setup of the SMFS experiments (see below), the simulations addressed only the K2, K3 and K4 domains, and did not allow us to obtain unfolding data for the two terminal K1 and K5 domains.

Steered molecular-dynamics simulations of the angiostatin mechanical unfolding under reducing conditions

The simulations showed that, when the three disulfide bonds of the ANG domains are fully reduced, the mechanical unfolding of K4 and K2, is controlled by the sequential rupture of two critical sets of interactions: first the hydrogen bonds sealing the C- to the N-terminal break, then a short antiparallel β-sheet ruptures (Figure 1). The failing of the three hydrogen bonds that sustain this β-sheet corresponds to the dominant peak in the simulated force–elongation profiles (Figure 2A) and to an energy barrier located at an elongation of $23\pm4\ \text{Å}$ from the fully folded, native structure. This peak is preceded by $13\pm2\ \text{Å}$ along the elongation coordinate by another peak or hump (Figure 2A), which is due to the rupture of the set of hydrogen bonds connecting the N and C termini. The structure of this intermediate is shown in Figure 3.
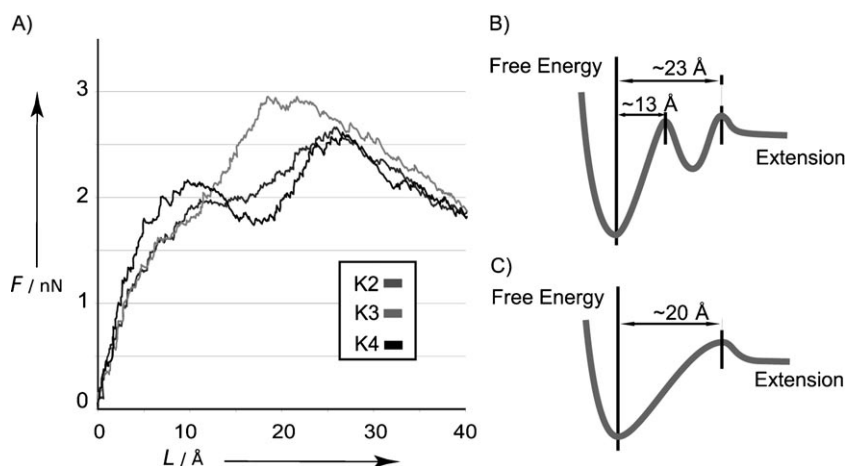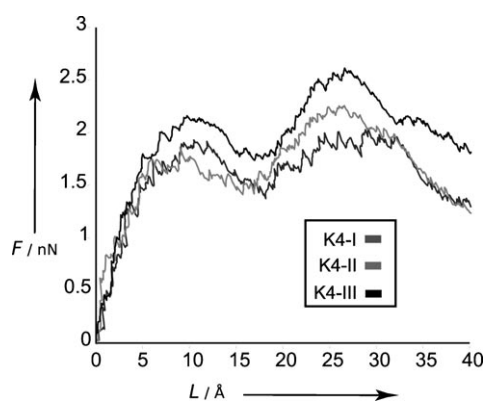

Figure 2. Force–elongation profiles of the A) K2, K3 and K4 ANG domains, and the corresponding B) double- or C) single-well free-energy landscapes that can be inferred from the SMD simulations on the K2–K4 or K3 domains.
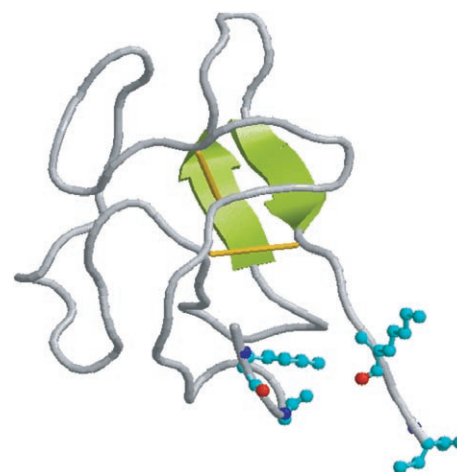
Figure 3. Structure of the partially unfolded and partially reduced intermediate that is mechanochemically populated in the K2 and K4 domains. The side chains evidenced are those involved in the hydrogen bonds between the N and C termini that break apart in the first unfolding step.

The SMD simulations were also performed on the partially reduced states of K2 and K4, in which their two internal Cys22–Cys61, and Cys50–Cys73 bonds are not reduced. As shown in Figure 4, their simulated force–elongation profiles do not substantially change with respect to the totally reduced state; the double humped profiles of Figure 2 are maintained, despite the topological blockades due to the unreduced disulfide bonds (see Figure 5). In conclusion the simulations showed that, when at least the most external Cys1–Cys78 bond is reduced, the mechanical unfolding of K2 and K4 is controlled by a double-well, free energy landscape like that shown in Figure 2B, which has a metastable intermediate, whose structure is depicted in Figure 3.

In the case of K3, the rupture of the five hydrogen bonds connecting the N and C termini and the failing of the β-sheet occurred without any relaxation into an intermediate in between. (see Figure 2A). The intertwining of these two ruptures in K3 is due to the greater number of hydrogen bonds con-

↖↖ These are not the final page numbers!

Figure 4. The double-humped force-elongation profiles obtained by SMD simulations of the K4 domains in the (I–III) reduction stages (see text). The double-well energy landscape inferred in Figure 2B for the completely reduced case therefore applies also to the other reduction stages.

necting its N and C termini: there are five instead of two or three, as in the case of K2 and K4, respectively. In the case of K3, the rupture of the fifth hydrogen bond takes place when the β-sheet is already under tension.

Stretching single angiostatin molecules under reducing conditions by the experimental SMFS methodology.

When single molecules of ANG are experimentally stretched by the SMFS methodology, force curves with sawtooth shaped peaks like that in Figure 6 are recorded. Therein, each peak corresponds to the unfolding of one single domain.

As demonstrated by a previous study,[18] the state of reduction of the relevant domain can be assigned to one of the three reduction stages based on the contour length increments of each peak with respect to the previous one: I (Cys1–Cys80 opened), II (Cys1–Cys80 + Cys22–Cys63 opened) and III (Cys1–Cys80 + Cys22–Cys63 + Cys51–Cys75 opened). This is made possible by the fact that as the reduction of the disulfide bonds proceeds, a larger portion of each module can unfold under the external force, and the distance between the peaks increases, as also shown by different authors in other proteins with internal disulfide bonds.[8, 9, 18, 26]

About 50% of the recorded peaks exhibit either a shoulder or a double tip at their crests, like that in Figure 6C–F. This statistic is maintained for all three reduction states. The length increment between the two tips, or between the tip and the shoulder, ranges from 10 to 20 Å, and their force is approximately equal (ratio 1st/2nd tip: 0.95 ± 0.15). Therefore, the profile of these double-tipped peaks matches the energy profile that results from the simulations, and is shown in Figure 2B for the K2 and K4 domains.
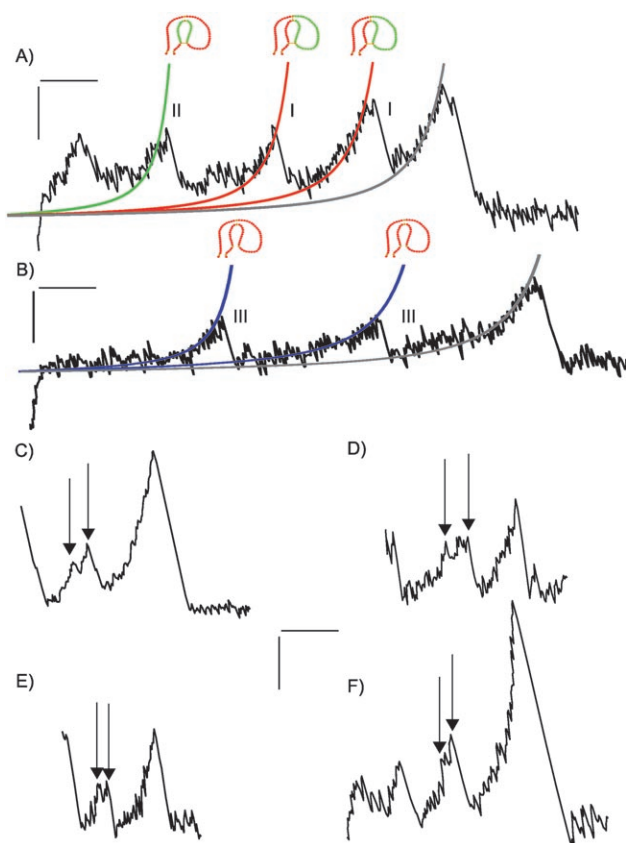
The assignment of these double-tipped peaks to K2 and K4 is confirmed by the frequency of their occurrence, which is in
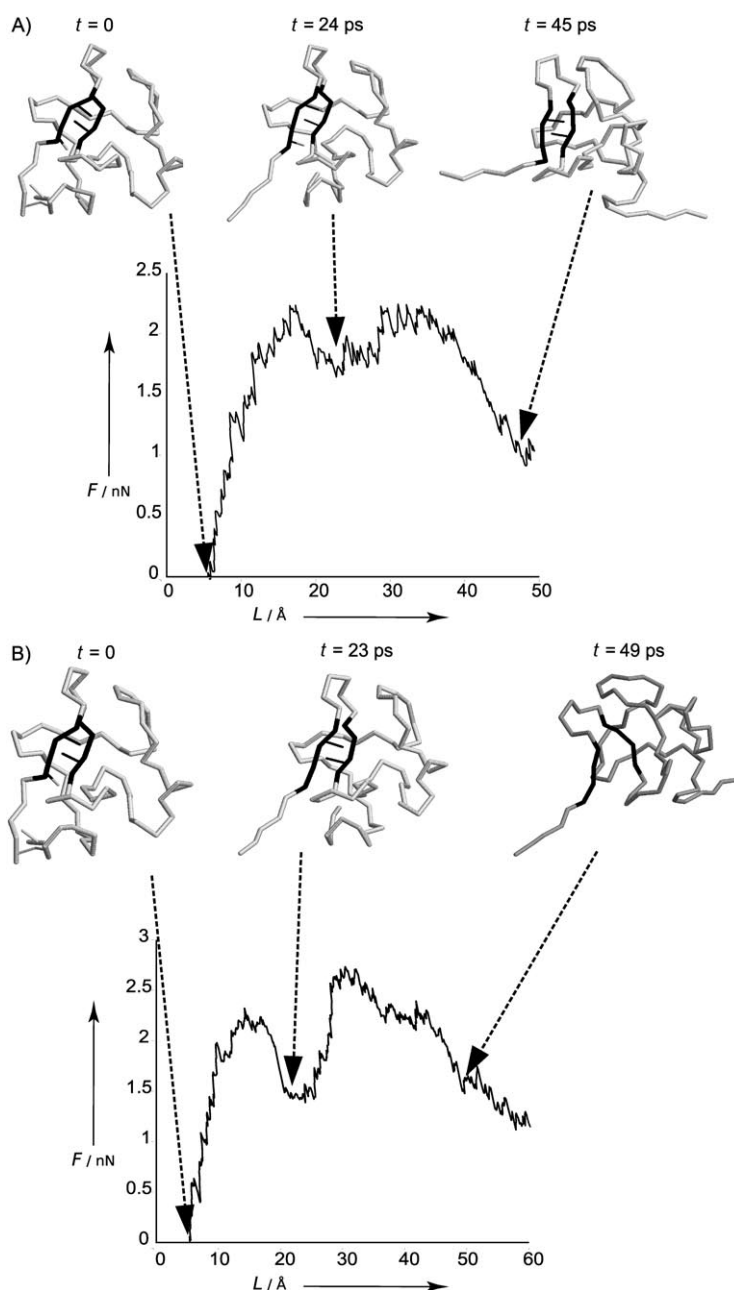
Figure 5. Snapshots of the SMD simulation of the mechanical unfolding of the K4 domain with A) only the most external disulfide bond unlocked (state I) B) all three disulfide bonds reduced (state III). In both cases the first barrier to mechanical unfolding is connected to the rupture of the hydrogen bonds between the N- and C-termini. The second barrier is due to the general disruption of the protein core. This takes place in B with the full unzipping of the β strands that is made possible by the reduction of all the three disulfide bonds. The S–S bridge in A allows only a distortion and twisting of the β-sheet. On the other hand, this distortion is sufficient to disrupt the core structure of the protein through its invasion by solvent.

accord with the expected mechanochemical population of the intermediate that was identified by the SMD simulations of those two domains. The other peaks with a single-tipped shape fit the case of K3, which according to the same simulations, should not have any on-path intermediate.

Our previously reported study on this molecule[18] was performed by pulling the ANG molecules deposited on a polystyr-

These are not the final page numbers! ↗↗

support the energy landscape depicted by the SMD simulations. We recorded and analyzed about a thousand force curves under different reducing conditions and at different pulling speeds (from 100 nm s^{-1} to 5600 nm s^{-1}). All the peaks were then assigned to the I, II, or III state of reduction (see Experimental Section, and Figure 7), and each data set, corre-
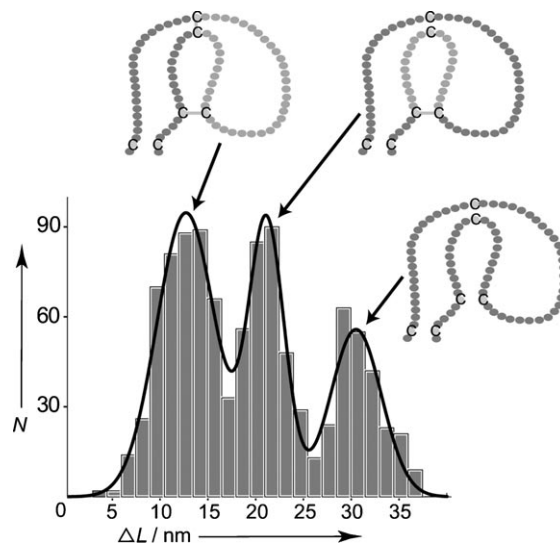
Figure 7. A triple Gaussian function with three peaks centered at 12.5, 21 and 30 nm fits the distribution of the unfolding length increments of the unfolded domains, obtained from the contour length increment of each single peak with respect to the previous one. According to Bustanji et al.[18] these values are in good agreement with the unfolding lengths expected for the three (I–III, see text) thiol–disulfide reduction stages (about 13.5, 20 and 28 nm). These stages are sketched on the top of each relative band with the portion of the domain accessible to mechanical unfolding (and, therefore, corresponding to the observed average length increment) shaded in dark gray.


Figure 6. A) and B) Typical ANG force–elongation curves (black) recorded by AFM-based single-molecule force spectroscopy. The worm-like chain lines are colored according to the state of reduction (I, II and III) that can be assigned to each unfolding peak. The last peak of all curves is the detachment peak (fit line in gray). The corresponding unfolded portion of the kringle domain is colored in red in the 2D sketches over the fitting lines. C) to F) Unfolding curves showing typical double-tipped unfolding peaks (arrows) revealing the population of the on-path intermediate predicted by SMD simulations with the structure reported in Figure 3. Scale bars (in the center) are 100 pN (vertical) and 10 nm (horizontal). The last peak of each curve is the detachment peak. The large vertical portion visible at the left of C, D and E is the final part of the unspecific adhesion signal, and is not related to protein unfolding. All the scale bars are 100 pN (vertical) and 10 nm (horizontal).

ene surface at one velocity only. We have now modified the methodology of sample preparation and have adopted the so-called dynamic approach of the SMFS methodology.[24,27–29] In fact, when a pulling force is applied to a folded protein, the dominant energy barrier that confines the folded structure is lowered. The most probable unfolding force therefore decreases with increasing applied force.[27,28,30] The decrease of the force depends on the pulling velocity, that is, on the loading rate of the external force. The dynamic approach of the SMFS methodology is based on the study of this dependence.[24,27–29] This methodology makes it possible to locate the dominant barrier and estimate the folding lifetime extrapolated at zero force.

Normally the SMD simulations are used to provide an atomistic interpretation for the experimental SMFS force extension data. In this case, due to intrinsic limitations of these data (see below), the SMFS dynamic approach data have been used to

sponding to each state was analyzed separately. For each pulling velocity, a histogram like that in Figure 7 was obtained, and the most probable unfolding forces, corresponding to each of the three peaks, that is, to each different reduced stage, were reported vs. the natural logarithm of the loading rate (Figure 8).

For the reduction stage III, an energy barrier at an extension of 16±8 Å (as shown in Figure 8B) was mapped from the slope of the linear dependences of the force upon the loading rate (Figure 8A). The fit of the experimental unfolding data by Monte Carlo simulations[31] confirmed the value of the energy barrier position, and estimated a lifetime, extrapolated at zero force, of the order of 10^{10} s, which is consistent with those reported for domains with β-sheet structures.[32] This 16±8 Å position most likely results from the limited capability of the dynamic SMFS to resolve the two barriers that were found by the SMD simulations, and to confine the intermediate identified in K2 and K4 at about 10 and 23 Å. This lack of resolution of the SMFS data is likely due to the intrinsic limitations we have met in the curve analysis, which come from the dissimilar structures of the domains.

↖↖ These are not the final page numbers!
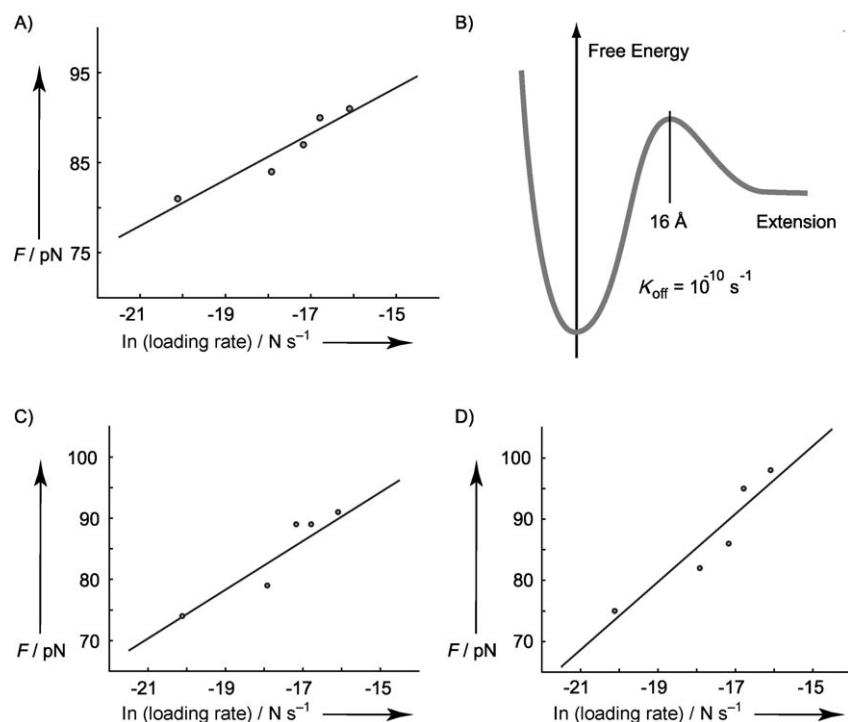
Figure 8. According to the dynamic approach of the SMFS methodology, the most probable unfolding forces that correspond to the kringle domains in their three reduction stages (I, II and III) were reported vs. the natural logarithm of the loading rate in A (stage III), C (stage I) and D (stage II). The energy landscape extrapolated from the plot in A is sketched in B.

The dynamic-force spectroscopy analysis for the reduction states I and II (see Figure 8 C and D) locates the barrier at extensions of 10 ± 8 and 8 ± 4 Å, respectively. The barrier position is therefore almost cut in half when the reduction of the disulfide bonds is not complete. The simulations suggest that, in the reduction states I and II, the β structure is partially blocked by the two internal S—S bonds (Cys22–Cys61, and Cys50–Cys73; see Figure 1), and the nature of the second and final unfolding barrier is markedly different from that of state III: the strands of the β-sheet are not fully broken apart, as in the case of that latter state, but rather distorted, with the residues 14–22 fully exposed to the solvent (see Figure 5).

In conclusion, we should expect that when a molecule of this protein experiences a force, once at least the Cys1–Cys78 disulfide bridge has been reduced, an intermediate becomes populated in the K4 and K2 domains (Figure 3). This structure does not correspond to any intermediate in K3.

Stretching ANG in a condition that mimics the redox environment met by this protein on the surface of a tumor cell.

The physiological significance of the states and the structures identified by the above study of the unfolding energy landscapes of the different reduction states of ANG domains, with regard to their antiangiogenic activity, is linked to the possibility that the same protein experiences in vivo the conditions that are required to reach them. We therefore translated the SMFS experiments to conditions mimicking the in vivo environ-

ments that this protein experiences on the surface of a tumor cell.

Due to the absence of in vivo studies, and because of the extreme difficulty of assigning a reduction state in that environment, there is considerable experimental uncertainty on the physiological reduction state of angiostatin kringle domains. We have seen how the SMFS can make this kind of assignment possible[18] in vitro, but not under in vivo conditions. We therefore carried out SMFS in vitro experiments aimed at reproducing the redox environment that is possibly met by ANG on the surface of a tumor cell.

Human thioredoxin (hTRX) is a widespread disulfide reductase present in the extracellular space[10] and it is active in altering the thiol–disulfide equilibrium of cell surface proteins.[33,34] Its reducing activity is ensured by the concurrent extracellular secretion of thioredoxin reductase (TRXR).[35] Furthermore TRX is greatly overexpressed on the surface of highly metastatic tumors.[36,37]

We performed the pulling experiments after having treated ANG with hTRX at a concentration of 20 μM, which is of the same order of magnitude as that found on the surface of mammalian tissues.[37] After this treatment, we blocked the reduced state by treating the sample with iodoacetamide. Force curves with the characteristic sequence of saw-tooth peaks, like those previously obtained with DTT (see Figure 6) were obtained. From the length increments in the force curves recorded after the treatment with hTRX, the statistical distribution of the reduction stage of each unfolded kringle domain was obtained (see Figure 9). This histogram demonstrates that under those conditions, this enzyme almost selectively reduces the Cys1–Cys78 disulfide bond. The coupling of this reducing enzyme to mechanical stress can therefore lead to the intermediate structure of Figure 3.

This result strongly indicates that the ANG kringle domains can be present in vivo, not only with their native, fully oxidized and folded structure, but also with a series of partially reduced and partially unfolded structures, including that in Figure 3. If we empirically assume that these structures can act as the antiangiogenic active forms of this protein rather than the native one, as commonly believed so far, a set of puzzling activity data can be accounted for, which has been so far unexplained. As explained in the following two paragraphs, one can both explain by using this assumption the triggering mechanism of the cell antimigratory activity of several fragments of ANG, and

These are not the final page numbers! ↗↗
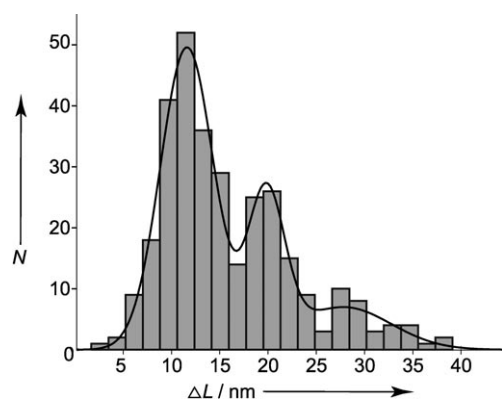
Figure 9. The distribution of the unfolding contour lengths obtained by mechanically unfolding ANG previously incubated with human thioredoxin. The peak at 12 nm fits the estimated 13.4 nm elongation that corresponds to the reduction of the Cys1–Cys78 disulfide bond only.

propose a cooperative binding mechanism of ANG to the endothelial cell surface ATPase.

Mechanochemical tuning of the binding of ANG with ATPase.

The binding of ANG K1–K5 with the endothelial cell surface ATPase has been recently proposed to mediate its antiproliferative activity by triggering caspase-mediated endothelial cell apoptosis activation.[38] A simple structural rationale for the binding of ANG to a single ATPase α-helix has been proposed by Geiger and Cnudde.[16] The docking was based on the kringle's ability to bind α-helices.[12,16,40] According to these authors the binding could be sustained by the interactions between exposed helices in the α and β subunits of ATPase, and the surface containing the LBS binding sites of the kringle domains.

By performing docking simulations[39] between ATPase, and a stretched and partially reduced (see below) ANG K2–K3 fragment, we found that a cooperative binding between ATPase and adjacent kringle domains can be settled. An increased binding affinity should result from this mechanically-induced, two-site interaction (see legend of Figure 12). The simulations showed that when the K2–K3 fragment is stretched, once its external disulfide bond has been reduced, its elongation takes place first at the expense of K3 only (Figure 10). K2 starts unfolding only after the opening of K3, and then reaches the intermediate conformation described above (see Figure 3). In this elongated structure of K2–K3, the Glu221 and Arg220 residues of K2 are at an average distance of 51 Å from the Asp309 and Lys311 of K3 (Figure 10).

The 51 Å distance makes it possible to those two ANG sites to bind in concert to the residues Lys496–Glu499 in chain A and Lys472–Asp471 in chain E of F1-ATPase (Figure 11 A and Figure 12). Those ANG binding sites are instead only 12 Å apart in the native structure of the K2–K3 fragment,[12] thus preventing its concerted binding to ATPase to take place.
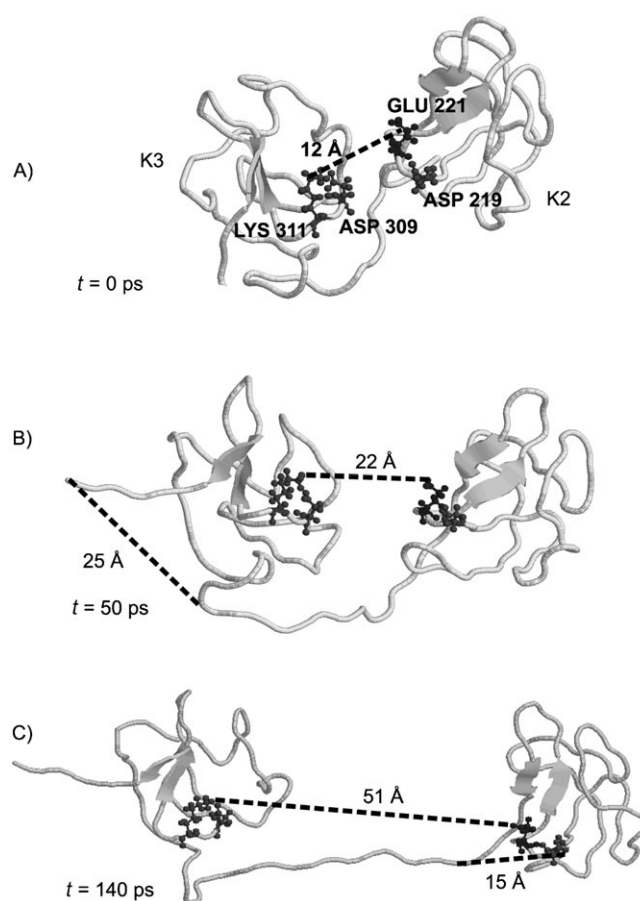

Figure 10. Mechanically stretching the K2–K3 fragment. SMD simulations show that when the K2–K3 fragment with the Cys1–Cys78 disulfide bonds reduced in both domains is mechanically stretched, the unfolding starts in K3 first (A). The five hydrogen bonds connecting the C and N termini are broken first. Afterwards, because of the rotation of one of the two strands of the β-sheet with respect to the other, the three hydrogen bonds that sustain this sheet fail (B). The unfolding of K2 starts at this point and reaches the conformation of its intermediate (C). In the meantime the conformation of K3 remains almost unchanged with respect to that in (B). The folding of the two more internal topological loops of the two domains is prevented by the Cys22–Cys61 and the Cys50–Cys73 disulfide bonds, which are not reduced. The preserved integrity of the folding of most sections of the two domains is confirmed by the RMSD values of the structures of the K2 and K3 domains as in (C), with respect to their native structures: 0.8 Å and 2.2 Å, respectively. The resolution of the structure (1KI0) used in the simulations is in fact of the same order of magnitude as these two values.

Mechanochemical tuning of the exposure of the K4 fragments with the highest antimigratory activity.

The binding of ANG to an ectopic, plasma membrane form of ATPase, is one of the mechanisms postulated for its antiangiogenic activity, even if certainly not the only one.[14,16,38] By the same mechanically induced elongation process that can make it possible for the K2–K3 fragment to settle a two-site binding to F1-ATPase, the metastable intermediate of the K4 domain (see Figure 3) becomes thermally populated. This intermediate can account for a set of puzzling data on the cell antimigratory activity of several fragments of ANG.

Among its five kringle domains, K4 is the one with the highest activity,[41] and its linear K4-A and cyclic K4-C fragments

↖↖ **These are not the final page numbers!**
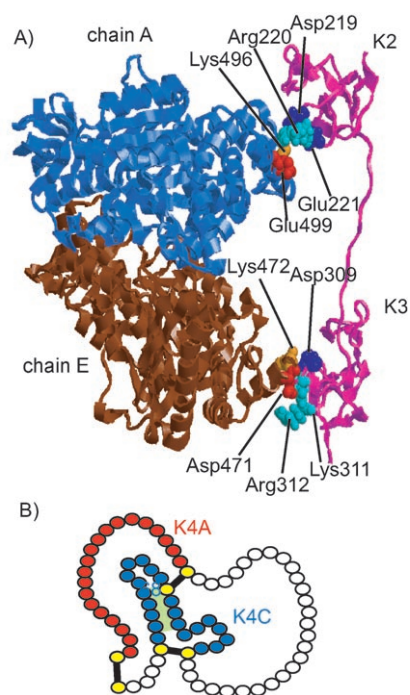
Figure 11. A) Mechanochemically induced binding of the β subunit (in blue) and the α subunit (in brown) of the F1-ATPase with the K2–K3 fragment (in magenta), which was elongated according to the energy landscapes in Figure 2 B and C, and the structure in Figure 10. Amino acid numbering refers to the crystal structures used in the simulation. B) Topology of the K4 domain that indicates the fragments (K4-A: red and K4-C: blue) whose antimigratory activity is higher than that of the full domain, according to ref.[42]
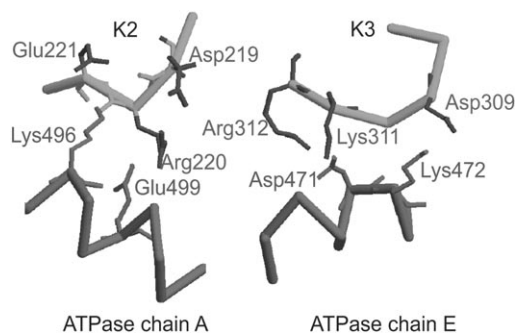
Figure 12. Binding energies and specific interactions that sustain the K2 and K3 binding to ATPase. The two most critical amino acid binding determinants of the docking showed in Figure 11 A are for K2: Glu221–Lys496, and Arg220–Glu499, whereas for K3 they are: Asp309–Lys472, Asp471–Lys311, and Asp471–Arg312. The K2 and K3 amino acids are numbered following the 1KI0 structure in the Protein Data Bank; the ATPase amino acids are numbered following the 1BMF structure in the PDB. The docking energies were calculated according to S. Liu et al.[55] Binding energy values of −4.99 and −5.20 Kcal mol^{-1} were obtained for the interaction of ATPase with K2 or K3 in their native structure, respectively. When a K2–K3 fragment is in its native form, only one of those two interactions can be settled: either with K2 or with K3. When K2–K3 is instead in the elongated form shown in Figures 10 C and 11 A, its binding to ATPase can be sustained by the interactions with both domains. The single binding-energy values were found to increase to −5.14 and −5.61 Kcal mol^{-1} for K2 and K3 respectively, leading to an overall estimated binding energy of −10.75 Kcal mol^{-1}. In conclusion, the elongation of the K2–K3 fragment not only increases the ANG–ATPase binding affinity, by making possible a concerted binding of both domains, but it also increases the binding affinity of each of them.

showed even higher activity than the entire K4 domain[42] (Figure 11 B). These two fragments are partially buried in the native structure of the kringle. In the intermediate form, however, the opening of the C–N termini ensures accessibility to the most active linear fragment K4-A, and to the K4-C loop. It should be mentioned, that the looped conformation of the K4-C fragment, which is apparently required for its antimigratory activity, is in this intermediate that is preserved by the integrity of both the β-sheet and the other two Cys22–Cys61 and the Cys50–Cys73 disulfide bonds (see Figures 3 and 10). We should therefore expect that whenever the reduction has gone beyond the rupture of these latter disulfide bonds, a decrease in activity might result. This prediction is confirmed by the activity data reported by Ji et al. .[41]

Conclusion

In conclusion, the SMFS experiment carried out with hTRX indicates that the ANG kringle domains can be present in vivo not only in their native, fully oxidized and folded structures, but with a series of partially reduced and partially unfolded structures, including that of the intermediate in Figure 3. We propose that these structures act as the active antiangiogenic forms of this protein, rather than the native one, as commonly believed so far. In Figure 13 a model is proposed for the mechanochemical control of the triggering of antiproliferative and antimigrative activities of ANG through the production of those partially reduced and partially unfolded structures. This model follows closely a general model for the combined action of redox and mechanical switches that we have recently hypothesized.[43]

The mechanochemical paradigm proposed here has broad implications for redox biology. It applies in particular to other kringle fragments of multimodular proteins, like prothrombin, apolipoprotein(a) and hepatocyte growth factor, whose role in angiogenesis has been proved.[14, 44] Moreover it also applies to the main components of the basement membrane-like thrombospondin-1, laminin or perlecan, which, like ANG, are composed of independent modules containing internal disulfide bonds[45–47] and experience mechanical stresses in vivo.

Experimental Section

Force spectroscopy experiments with DTT. A drop of purified angiostatin K1–5 (ANG; Calbiochem) solution (20 μL, 0.5 μM) in HEPES buffer (pH 7.4), previously incubated with DTT (100 mM; 2 h, 37 °C; which is more than enough to reduce all kringle disulfide bonds[18, 48]) was deposited on a clean glass surface that had been rinsed with water, acetone and ethanol, drawn through a Bunsen flame and rinsed again. In the previous paper[18] we used a polystyrene surface as a substrate for the deposition of ANG. We switched to glass to avoid possible artifacts due to the possible pulling of polystyrene chains from the surface.

After a deposition time of 30 min, the sample was then inserted into a fluid cell. The force spectroscopy experiments were performed in micro filtered PBS buffer with DTT (100 mM) with a Nanoscope IIIa multimode atomic force microscope (AFM; Digital Instruments) using sharpened silicon nitride (Si$_3$N$_4$) tips (from Park

These are not the final page numbers! ↗↗
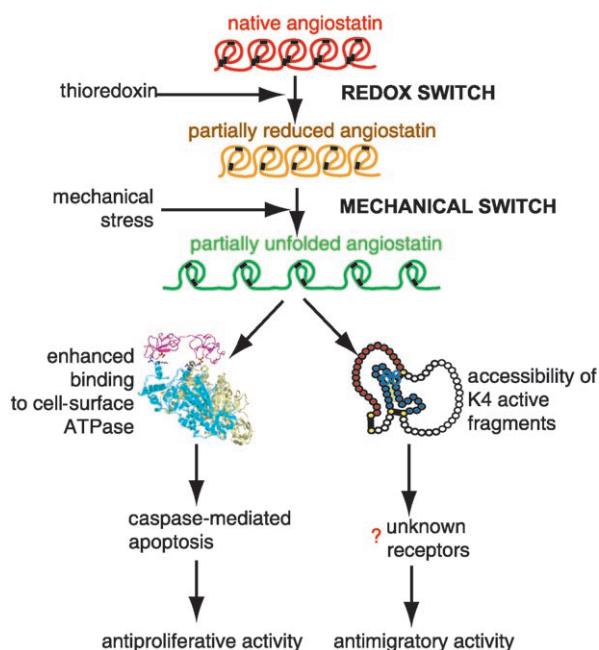
Figure 13. An example model of how force and oxidation state can work in tandem for an enhanced antiproliferative and antimigratory activity of ANG. The reducing environment met by ANG on the surface of highly metastatic tumors[36,37] is able to reduce the most external disulfide bonds of its kringle domains. This reduction creates the possibility that the mechanical stress that is constantly being developed in the ECM environment, where ANG is located,[11] can mechanically unfold a topological loop of 40 amino acids. The resulting partially elongated, and partially unfolded structure of ANG (see Figure 3) can activate new binding capabilities and trigger new biochemical signals, as shown for the cases of a K2–K3 fragment and the K4 kringle domain. The hierarchical activation of those two switches can lead i) to an enhanced binding of a K2–K3 fragment to ATPase and therefore to an increased antiproliferative activity of ANG (see Figure 11 A); ii) to a more efficient exposure of the two segment chains that ensure, through the interaction with still unknown receptors, antimigratory activities higher than that of the native K4 full domain (see Figure 11 B).

Scientific), at room temperature. Cantilever spring constants were measured by their thermal spectrum (range between 40 and 60 pN nm^{-1}). The loading rate values reported in Figure 8 were computed by taking into account that they are related to the pulling speed through the elasticity of the bridge, which is composed of by both the molecule under stress, and the AFM cantilever. After analyzing the experimental data,[49] we estimated that an equivalent spring constant of 27 ± 3 pN nm^{-1} can be assigned to the bridge for the speed range that we used.

Force spectroscopy experiments with thioredoxin. ANG (0.13 μM) was incubated for 30 min at 37 °C with an activated human thioredoxin (hTRX; from Calbiochem) solution (20 μM, ANG/hTRX molar ratio about 1:150). After the reduction, ANG was alkylated for 30 min in the dark by adding iodoacetamide (from Fluka) at a 5–10 mM final concentration in order to avoid the oxidation of hTRX-reduced Cys residues, and to block hTRX activity. ANG was finally purified from hTRX and iodoacetamide by using YM-30 ultra free Microcon (from Millipore; 4 °C). We found that this simple purification step was enough to avoid interference in the force spectroscopy experiments, due to engagements of the residual hTRX rather than ANG molecules. One drop of the final solution (0.5 μM) was used for the force spectroscopy experiments, following the protocol described above, but without DTT in the fluid–cell buffer.

The activation of the enzymatic site of hTRX was obtained by incubation with DTT (from Sigma–Aldrich; 1 h, 37 °C, 1 mM) in HEPES buffer (pH 7.4). The activated hTRX was purified by using YM-3 ultra free Microcon (from Millipore) at 4 °C (final DTT concentration below 50 μM). Control force spectroscopy experiments performed with DTT at 50 μM ruled out any detectable reduction of ANG, which would have been contributed by the DTT.

Force spectroscopy raw data analysis. The unfolding force curves were selected by keeping only those clearly presenting the sawtooth profile that is characteristic of angiostatin single-molecule mechanical unfolding for analysis.[18] More specifically, the measured curves showed a) from 2 to 4 peaks (1–3 unfolding peaks plus final detachment); b) peaks whose height was similar besides the case of the last peak that must be the highest (or at least as high as the others); c) no indication of plateaus or other features superimposed on the sawtooth profile.

We observed no significant evidence of the two-stage unfolding described for disulfide-bonded domains,[8] probably because in our case the disulfide bonds are already naturally accessible to the solvent; however we cannot completely rule out that some sporadic occurrence of these effects might have entered our statistics.

The selected curves have been analyzed by a custom MatLab program which performs a double-parameter fit on each unfolding peak. The fit function is a worm-like chain,[50] and the two fitted parameters are the persistence length (range of variation from 3.5 to 7 Å) and the contour length. The fit is not normally performed on the entire peak profile: it is advisable in fact to exclude the final part of the peak, because it can be affected by small enthalpic deviations from the entropic elasticity profile. The implemented analysis software allows one to directly select the fit interval on the curve plot.

Dynamic single-molecule force spectroscopy analysis. The single unfolding peaks have then been separated into three classes according to their contour length increase: I (12.5 ± 4 nm), II (21 ± 2.5 nm) and III (30.5 ± 3 nm), according to their triple Gaussian distribution (see Figure 7). Only the peaks that belonging to one of these three classes have been used for dynamic SMFS analysis. For the amount of data used for each class, see the Supporting Information.

Monte Carlo simulations: Monte Carlo simulations of the stretching experiments were performed according to a previously published procedure.[23] See the Supporting Information for details.

Steered molecular dynamics simulations. SMD simulations were performed according to ref.[19] The kringle domain was solvated with the TIP3 water model, and the energy of the system was minimized. After this, the kringle–water box was heated over 10 ps and then equilibrated with a thermal bath at 300 K for another 10 ps. The SMD simulation was performed with a time step of 1 fs, a uniform dielectric constant of 1, and a cut-off of Coulumb forces with a switching function from 10–13 Å. The molecular dynamics were carried out using the CHARMM19 force field, and by fixing the C-α atom of one terminus and applying an external force to the other C-α terminus. For each kringle, 5 different simulations were performed at 1 Å ps^{-1} pulling speed. The pulling direction was chosen along the vector from the fixed atoms to pulled one. The value of the spring constant k was set to 10 K_BT Å^{-2}, corresponding to the thermal fluctuation of constrained C-α at 300 K. Simulations with these values of k and v correspond to pulling with a stiff spring in the drift regime. The K2 and K3 structures have been extracted from the human K1–3 protein structure[12] (PDB ID: 1KI0, http://

www.rcsb.org); the K4 structure from the structure labeled 1KRN in the PDB.[51] The SMD simulations were carried out with NAMD 2.5,[52] and the solvated kringle domains were obtained by using the TIP3 water model with the GROMACS 3.0 program.[53] Both programs were executed on a double processor Intel Xeon 2.4 GHz machine with the Debian GNU/Linux operating system.

Protein–protein docking simulation. According to the procedure described in the previous section, the crystal structure of K1–3, with only one disulfide bond reduced for each kringle, was solvated in water and its energy minimized. The whole system was heated and equilibrated at 300 K and then a SMD simulation of 500 ps was performed. For the docking procedure, only a fragment of the K2–3 of 1KI0 structure was considered. The stretched K2–K3 fragment was obtained after 140 ps of steered molecular dynamic simulation. The two subunits of F1 ATPase were extracted selecting the chains A and E of the crystal structure labeled 1BMF in the PDB.[54] Docking of the ANG fragment to the ATPase was performed by using Z-DOCK.[39] Patches of 10 Å radius centered on the relative binding sites were considered.

Acknowledgements

[1] G. Bao, S. Suresh, *Nat. Mater.* **2003**, *2*, 715.
[2] C. Bustamante, Y. R. Chemla, N. R. Forde, D. Izhaky, *Annu. Rev. Biochem.* **2004**, *73*, 705.
[3] G. Baneyx, L. Baugh, V. Vogel, *Proc. Natl. Acad. Sci. USA* **2002**, *99*, 5139.
[4] I. Tinoco, Jr., C. Bustamante, *Biophys. Chem.* **2002**, *101–102*, 513.
[5] M. Osawa, M. Masuda, K.-i. Kusano, K. Fujiwara, *J. Cell Biol.* **2002**, *158*, 773.
[6] V. Vogel, W. E. Thomas, D. W. Craig, A. Krammer, G. Baneyx, *Trends Biotechnol.* **2001**, *19*, 416.
[7] P. J. Hogg, *Trends Biochem. Sci.* **2003**, *28*, 210.
[8] N. Bhasin, P. Carl, S. Harper, G. Feng, H. Lu, D. W. Speicher, D. E. Discher, *J. Biol. Chem.* **2004**, *279*, 45865.
[9] A. P. Wiita, S. R. Ainavarapu, H. H. Huang, J. M. Fernandez, *Proc. Natl. Acad. Sci. USA* **2006**, *103*, 7222.
[10] A. Rubartelli, A. Bajetto, G. Allavena, E. Wollman, R. Sitia, *J. Biol. Chem.* **1992**, *267*, 24161.
[11] T. Ohashi, D. P. Kiehart, H. P. Erickson, *Proc. Natl. Acad. Sci. USA* **1999**, *96*, 2153.
[12] M. C. Abad, R. K. Arni, D. K. Grella, F. J. Castellino, A. Tulinsky, J. H. Geiger, *J. Mol. Biol.* **2002**, *318*, 1009.
[13] M. S. O'Reilly, L. Holmgren, Y. Shing, C. Chen, R. A. Rosenthal, M. Moses, W. S. Lane, Y. Cao, E. H. Sage, J. Folkman, *Cell* **1994**, *79*, 315.
[14] Y. Cao, R. Cao, N. Veitonmaki, *Curr. Med. Chem. Anti-Cancer Agents* **2002**, *2*, 667.
[15] T. Mogues, M. Etzerodt, C. Hall, G. Engelich, J. H. Graversen, K. L. Hartshorn, *J. Biomed. Biotechnol.* **2004**, *2004*, 73.
[16] J. H. Geiger, S. E. Cnudde, *J. Thromb. Haemostasis* **2004**, *2*, 23.
[17] N. Q. Balaban, U. S. Schwarz, D. Riveline, P. Goichberg, G. Tzur, I. Sabanay, D. Mahalu, S. Safran, A. Bershadsky, L. Addadi, B. Geiger, *Nat. Cell Biol.* **2001**, *3*, 466.
[18] a) Y. Bustanji, B. Samorì, *Angew. Chem.* **2002**, *114*, 1616–1618; *Angew. Chem. Int. Ed.* **2002**, *41*, 1546–1548.
[19] H. Lu, B. Isralewitz, A. Krammer, V. Vogel, K. Schulten, *Biophys. J.* **1998**, *75*, 662.
[20] M. Rief, H. Grubmüller, *ChemPhysChem* **2002**, *3*, 255.
[21] D. J. Brockwell, D. A. Smith, S. E. Radford, *Curr. Opin. Struct. Biol.* **2000**, *10*, 16.
[22] M. Carrion-Vazquez, A. F. Oberhauser, T. E. Fisher, P. E. Marszalek, H. Li, J. M. Fernandez, *Prog. Biophys. Mol. Biol.* **2000**, *74*, 63.
[23] R. B. Best, J. Clarke, *Chem. Commun.* **2002**, 183.
[24] Y. Bustanji, C. R. Arciola, M. Conti, E. Mandello, L. Montanaro, B. Samori, *Proc. Natl. Acad. Sci. USA* **2003**, *100*, 13292.
[25] B. Samori, G. Zuccheri, P. Baschieri, *ChemPhysChem* **2005**, *6*, 29.
[26] P. Carl, C. H. Kwok, G. Manderson, D. W. Speicher, D. E. Discher, *Proc. Natl. Acad. Sci. USA* **2001**, *98*, 1565.
[27] E. Evans, *Annu. Rev. Biophys. Biomol. Struct.* **2001**, *30*, 105.
[28] H. Dietz, M. Rief, *Proc. Natl. Acad. Sci. USA* **2004**, *101*, 16192.
[29] R. Ros, R. Eckel, F. Bartels, A. Sischka, B. Baumgarth, S. D. Wilking, A. Puhler, N. Sewald, A. Becker, D. Anselmetti, *J. Biotechnol.* **2004**, *112*, 5.
[30] C. Cecconi, E. A. Shank, C. Bustamante, S. Marqusee, *Science* **2005**, *309*, 2057.
[31] M. Rief, J. M. Fernandez, H. E. Gaub, *Phys. Rev. Lett.* **1998**, *81*, 4764.
[32] D. J. Brockwell, G. S. Beddard, J. Clarkson, R. C. Zinober, A. W. Blake, J. Trinick, P. D. Olmsted, D. A. Smith, S. E. Radford, *Biophys. J.* **2002**, *83*, 458.
[33] L. J. Matthias, P. T. Yam, X. M. Jiang, N. Vandegraaff, P. Li, P. Poumbourios, N. Donoghue, P. J. Hogg, *Nat. Immunol.* **2002**, *3*, 727.
[34] M. Kwon, C. S. Yoon, W. Jeong, S. G. Rhee, D. M. Waisman, *J. Biol. Chem.* **2005**, *280*, 23584.
[35] A. Soderberg, B. Sahaf, A. Rosen, *Cancer Res.* **2000**, *60*, 2281.
[36] D. T. Lincoln, E. M. Ali Emadi, K. F. Tonissen, F. M. Clarke, *Anticancer Res.* **2003**, *23*, 2425.
[37] G. Powis, W. R. Montfort, *Annu. Rev. Biophys. Biomol. Struct.* **2001**, *30*, 421.
[38] N. Veitonmaki, R. Cao, L. H. Wu, T. L. Moser, B. Li, S. V. Pizzo, B. Zhivotovsky, Y. Cao, *Cancer Res.* **2004**, *64*, 3679.
[39] R. Chen, L. Li, Z. Weng, *Proteins* **2003**, *52*, 80.
[40] J. L. Rios-Steiner, M. Schenone, I. Mochalkin, A. Tulinsky, F. J. Castellino, *J. Mol. Biol.* **2001**, *308*, 705.
[41] W. R. Ji, F. J. Castellino, Y. Chang, M. E. Deford, H. Gray, X. Villarreal, M. E. Kondri, D. N. Marti, M. Llinas, J. Schaller, R. A. Kramer, P. A. Trail, *FASEB J.* **1998**, *12*, 1731.
[42] M. Dettin, S. Bicciato, C. Scarinci, E. Cline, M. W. Lingen, C. Di Bello, *ChemBioChem* **2003**, *4*, 1238.
[43] M. Sandal, F. Grandi, B. Samori, *Polymer* **2006**, *47*, 2571.
[44] S. Sengupta, E. Gherardi, L. A. Sellers, J. M. Wood, R. Sasisekharan, T. P. Fan, *Arterioscler. Thromb. Vasc. Biol.* **2003**, *23*, 69.
[45] J. Lawler, R. Hynes, *J. Cell Biol.* **1986**, *103*, 1635.
[46] J. Stetefeld, U. Mayer, R. Timpl, R. Huber, *J. Mol. Biol.* **1996**, *257*, 644.
[47] B. Schulze, T. Sasaki, M. Costell, K. Mann, R. Timpl, *Matrix Biol.* **1996**, *15*, 349.
[48] M. Trexler, L. Patthy, *Biochim. Biophys. Acta* **1984**, *787*, 275.
[49] W. Dettmann, M. Grandbois, S. Andre, M. Benoit, A. K. Wehle, H. Kaltner, H. J. Gabius, H. E. Gaub, *Arch. Biochem. Biophys.* **2000**, *383*, 157.
[50] C. Bustamante, J. F. Marko, E. D. Siggia, S. Smith, *Science* **1994**, *265*, 1599.
[51] B. Stec, A. Yamano, M. Whitlow, M. M. Teeter, *Acta Crystallogr. Sect. D Biol. Crystallogr.* **1997**, *53*, 169.
[52] L. Kalé, R. Skeel, M. Bhandarkar, R. Brunner, A. Gursoy, N. Krawetz, J. Phillips, A. Shinozaki, K. Varadarajan, K. Schulten, *J. Comput. Phys.* **1999**, 283.
[53] E. Lindahl, B. Hess, D. van der Spoel, *J. Mol. Model.* **2001**, *7*, 306.
[54] J. P. Abrahams, A. G. Leslie, R. Lutter, J. E. Walker, *Nature* **1994**, *370*, 621.
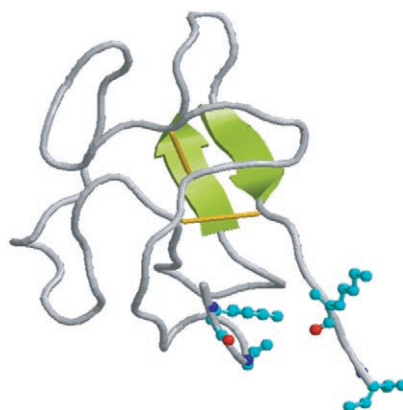[55] S. Liu, C. Zhang, H. Zhou, Y. Zhou, *Protein J.* **2004**, *56*, 93.

These are not the final page numbers! ↗↗

ARTICLES

F. Grandi, M. Sandal, G. Guarguaglini,
E. Capriotti, R. Casadio, B. Samorì*

■■ – ■■

**Hierarchical Mechanochemical
Switches in Angiostatin**

💻 **A novel protein signaling switch** based on the coupling of redox conditions and mechanical stresses upon a disulfide bond is reported. Single-molecule experiments and simulations on angiostatin (a protein with antitumor activity) indicate that this switching mechanism can control the access to partially reduced and partially unfolded structures (see figure); these are proposed herein to be the active forms of angiostatin, rather than the native one, as commonly believed so far.

↖↖ These are not the final page numbers!